Volume 2 | Number 17 | 7 May 2014 | Pages 5939–6248

Journal of Materials Chemistry A

Materials for energy and sustainability

www.rsc.org/MaterialsA

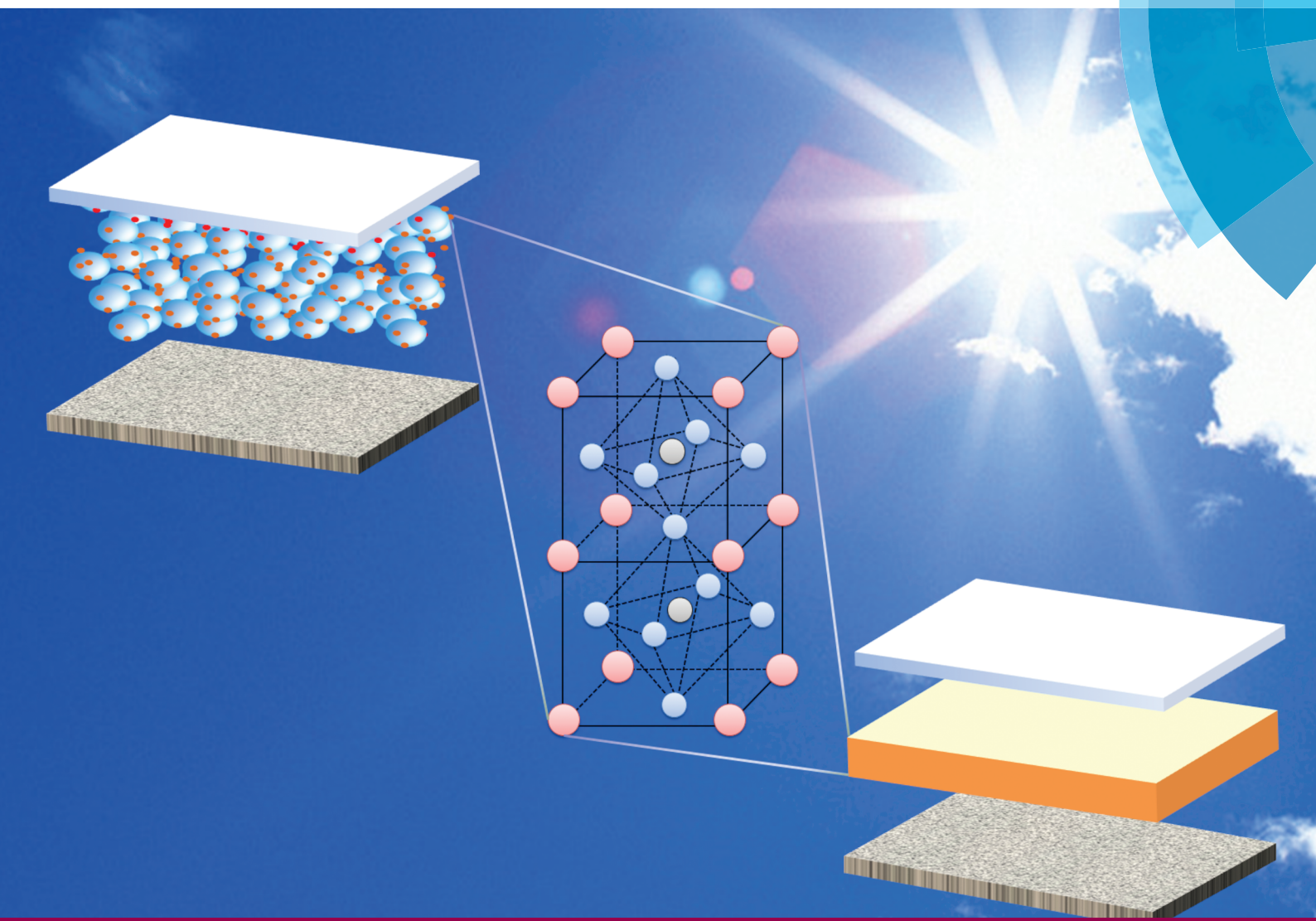

Themed issue: Emerging Investigators

ISSN 2050-7488

ROYAL SOCIETY OF CHEMISTRY

FEATURE ARTICLE

Zhiqun Lin *et al.*

High efficiency perovskite solar cells: from complex nanostructure to planar heterojunction

Journal of Materials Chemistry A

FEATURE ARTICLE

View Article Online
View Journal | View Issue

Cite this: J. Mater. Chem. A, 2014, 2, 5994

High efficiency perovskite solar cells: from complex nanostructure to planar heterojunction

Ming He,[a] Dajiang Zheng,[ab] Mengye Wang,[ab] Changjian Lin[b] and Zhiqun Lin*[a]

Received 16th October 2013
Accepted 1st November 2013

DOI: 10.1039/c3ta14160h

www.rsc.org/MaterialsA

Perovskite solar cells have garnered great attention in recent years as promising high performance next-generation solar cells with long-term stability at low cost. Since the seminal work of Miyasaka and others in 2009, the power conversion efficiency (PCE) of perovskite-based dye-sensitized solar cells (DSSCs) has rapidly increased from 3.8% to 15% over the past four years, exceeding the highest efficiency of conventional organic dye-sensitized DSSCs. Recently, the perovskite has been demonstrated to act successfully as an active layer in simple planar-heterojunction solar cells with no need of complex nanostructured DSSC architectures, leading to an attractively high PCE of 15.4% at a competitive low manufacturing cost. In this Feature Article, we aim to review the recent impressive development in perovskite solar cells, and discuss the prognosis for future progress in exploiting perovskite materials for high efficiency solar cells.

1. Introduction

Global energy demand has been continually increasing with industrial development and population growth in recent decades, especially for conventional energy resources such as fossil oil, coal and natural gas. To date, over 80% of energy consumption is generated from fossil fuels, which causes the environmental pollution and global-warming issues. More importantly, fossil fuels are non-renewable energy and will eventually be exhausted in the future. In this context, solar cells that convert solar energy into electrical energy possess cost-effective, reliable and safe attributes and present as one of promising renewable alternatives to fossil fuels.[1–8] Since the first practical solar cell was fabricated from a silicon p–n junction, silicon solar cells are currently leading the commercial photovoltaics markets with 80% share. The highest power conversion efficiency (PCE) of silicon solar cells is nearly 28%.[9] A very high purity (*e.g.*, ≥99.9999%) is often required for solar-grade silicon as the charge generation and transport in silicon is very sensitive to defects.[10] In addition, due to a large energy difference between the direct gap (~3.4 eV) and indirect gap (~1.1 eV) of silicon,[11] the active layer of silicon solar cells must be thick enough (*e.g.*, typically 300 μm) to efficiently absorb incident sunlight. This makes silicon solar cells expensive. To this end, thin-film solar cells composed of inorganic semiconductors with a direct bandgap are then explored,[12] including cadmium

[a]School of Materials Science and Engineering, Georgia Institute of Technology, Atlanta, GA 30332, USA. E-mail: zhiqun.lin@mse.gatech.edu

[b]Department of Chemistry, College of Chemistry and Chemical Engineering, Xiamen University, Xiamen 361005, China

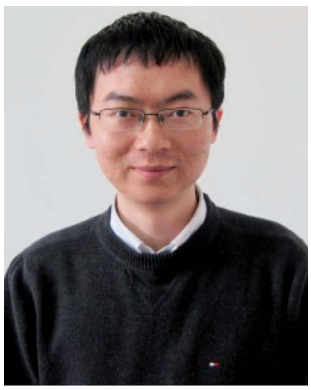

Ming He received his PhD degree in Polymer Chemistry and Physics from the Fudan University of China in 2011. Currently, he works as a postdoctoral fellow in Professor Zhiqun Lin's research group at the Georgia Institute of Technology. His research interests include conjugated polymers, block copolymers, quantum dots, polymer solar cells, dye-sensitized solar cells, graphene electrode materials, and thermoelectrical nanocomposites.

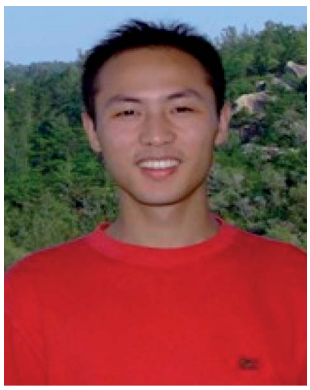

Dajiang Zheng is a PhD student in the College of Chemistry and Chemical Engineering at Xiamen University, China. He is currently a visiting PhD student in Prof. Zhiqun Lin's group at Georgia Institute of Technology. His research interests cover the synthesis of one-dimensional titanium dioxide, perovskite materials, and their applications in dye-sensitized solar cells.

telluride (CdTe),[13] copper indium gallium selenide (CIGS),[14] and copper zinc tin sulfide (CZTS).[15] The highest efficiency of 37.5% has been reported for InGaP/GaAs/InGaAs multijunction thin-film solar cells.[9] However, the manufacturing of inorganic thin-film solar cells usually involves costly, high temperature and high vacuum vapor deposition. Moreover, most of the thin-film solar cells to date contain elements that are toxic and of low abundance in the Earth, thereby limiting their mass production and widespread applications.

Dye-sensitized solar cells (DSSCs) have received considerable interest since the first report in 1991 by Grätzel and his coworkers,[16] due primarily to their excellent photovoltaic performance at a relatively low fabrication cost.[17] Unlike the classic solid-state junction device, the charge generation and transfer are separately processed in dyes and semiconductors in DSSCs, thereby forming a photochemical solar cell.[18] Notably, DSSCs can be assembled under normal pressure and temperature, which reduces the fabrication cost. Typically, a DSSC consists of a wide band-gap semiconductor as a photoanode (*e.g.*, TiO_2 with a bandgap, E_g, of 3.2 eV) for transferring and collecting electrons, a dye as a sensitizer (*e.g.*, ruthenium-based complex, N719) for absorbing solar photons, a liquid redox electrolyte (*e.g.*, iodide/triiodide couple) for deoxidizing oxidized dyes, and a platinum counter electrode for reproducing oxidized ions in the redox electrolyte (*e.g.*, iodide ion).[19–22] A PCE over 12% has been achieved using a porphyrin-sensitized mesoporous TiO_2 photoanode and a cobalt redox electrolyte,[10] wherein the electrons generated from photoexcited dyes are injected into the conduction band of the TiO_2 photoanode, while the concomitant holes are transferred through the redox electrolyte to the counter electrode. For conventional DSSCs using liquid electrolytes, the energy loss of solar-to-electricity conversion is largely related to the electron transfer from the sensitizer to the TiO_2 photoanode and the dye regeneration from the electrolyte.[23] The strategies to reduce the energy loss include: (1) rational design of dye molecules with their lowest unoccupied molecular orbital (LUMO) matching the quasi Fermi level of the TiO_2 photoanode, (2) optimization of the TiO_2 photoanode with nanostructured architectures for enhanced dye loading and electron transport, (3) exploitation of redox electrolytes with effective components for hole transport.[21,24–26]

Although the stability of DSSCs has been extensively evaluated in the lab, the long-term durability of semi-commercial DSSC products is still not very satisfactory, due mostly to the degradation of organic dyes and the leakage of liquid electrolytes after a long-time illumination.[27–29] To avoid the leakage of liquid electrolytes, increase the lifetime of devices, and reduce the manufacturing cost by dispensing with the need for device sealing, recent efforts have concentrated on the replacement of liquid electrolytes with solid-state electrolytes.[30–32] Amorphous organic hole-transport material (HTM), 2,2′,7,7′-tetrakis-(*N*,*N*-di-*p*-methoxyphenyl-amine)-9,9′-spirobifluorene (spiro-MeO-TAD), was initially introduced to substitute the iodide/triiodide liquid electrolyte, yet resulting in a low PCE of 1%,[33] which was attributed to the short diffusion length of charge carriers and the incomplete pore filling of mesoporous TiO_2 films. Recent advances in the synthesis of new dyes with enhanced extinction

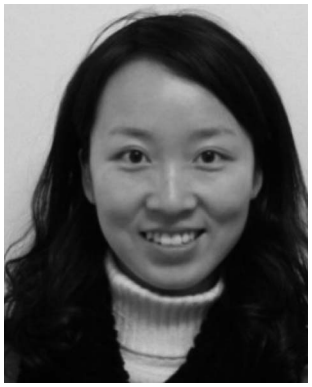

Mengye Wang is a PhD student in the College of Chemistry and Chemical Engineering at Xiamen University. She received her Bachelor of Science in Chemistry from Xiamen University in 2010. She is currently a visiting PhD student in Prof. Zhiqun Lin's group at Georgia Institute of Technology. Her research interests include the applications of TiO_2 in photocatalytic degradation of organic pollutants, water splitting and dye-sensitized solar cells.

Changjian Lin is a Professor in the State Key Laboratory of Physical Chemistry of Solid Surfaces, and College of Chemistry and Chemical Engineering at Xiamen University. He received his PhD in Physical Chemistry from Xiamen University in 1985. His research interests include electrochemical methods, corrosion and protection, biomaterials and biosurfaces, advanced materials for energies and environments, such as dye-sensitized and quantum dot-sensitized solar cells, photogenerated cathodic protection, surface wettability, water splitting hydrogen production and photocatalytic degradation of organic pollutants.

Zhiqun Lin is an Associate Professor in the School of Materials Science and Engineering at Georgia Institute of Technology. He received his PhD in Polymer Science and Engineering from the University of Massachusetts, Amherst in 2002. His research interests include polymer solar cells, dye-sensitized solar cells, semiconductor organic–inorganic nanocomposites, photocatalysts, quantum dots (rods), conjugated polymers, block copolymers, polymer blends, hierarchical structure formation and assembly, surface and interfacial properties, multifunctional nanocrystals, and Janus nanostructures. He is a recipient of an NSF Career Award.

coefficients render the increase of PCE of spiro-OMeTAD-based DSSCs to nearly 6.1%.[34]

Due to their excellent electrical conductivity, conjugated polymers such as poly(3-hexylthiophene) (P3HT), polyaniline, and polypyrrole have also been explored as potential alternatives to liquid electrolytes.[35,36] Unfortunately, the device performance of conjugated polymer electrolyte-based DSSCs is also limited owing to the poor filling of electrolytes within the mesoporous TiO_2 photoanode. A champion PCE of 3.8% was achieved in P3HT electrolyte-based DSSCs using organic dyes as sensitizers.[37] Interestingly, the efficiency of P3HT electrolyte-based DSSCs was then increased to over 5% by implementing inorganic Sb_2S_3 nanocrystals as sensitizers.[38] Compared to organic dyes, inorganic semiconductor nanocrystals offer expanded flexibility for serving as high-efficiency sensitizers, benefiting from their tunable optical properties,[8] high extinction coefficients,[39] and large intrinsic dipole moments.[40] Nevertheless, inorganic nanocrystal sensitizers still suffer from the relatively poor infiltration within mesoporous TiO_2 films, low charge carrier mobility, and fast carrier recombination,[41] and thus low device performance of DSSCs.

The breakthrough discovery of organometal halide perovskite $CH_3NH_3PbX_3$ (X = halogen) as high-efficiency light sensitizers in photoelectrochemical cells shed new light on developing low cost, high performance next generation solar cells.[42] Perovskite is named after Russian mineralogist Perovskite who first characterized the crystal structure of ABX_3-type (X = halogen, oxygen; *e.g.*, $CaTiO_3$) inorganics.[42–44] In $CH_3NH_3PbX_3$ nanocrystals, Pb^{2+} cations adopt the octahedral coordination of X^- anions together with the cuboctahedral coordination of $CH_3NH_3^+$ anions (Fig. 1a).[45] The electronic activities of $CH_3NH_3PbX_3$ nanocrystals are highly correlated with their crystalline structures. For example, the band gap of $CH_3NH_3Pb(I_{1-x}Br_x)_3$ ($0 \le x \le 1$) can be gradually tuned from ~1.2 eV to ~2.3 eV by adjusting the component ratio of Br^- anions (Fig. 1b), accompanied by the crystal structure transformation from the tetragonal structure of $CH_3NH_3PbI_3$ to the cubic structure of $CH_3NH_3PbBr_3$ as the smaller Br^- ion radius is relatively favorable for the formation of the cubic structure (Fig. 1c).[46] Similarly, the optical absorption of $CH_3NH_3Pb(I_{1-x}Br_x)_3$ ($0 \le x \le 1$) can be readily adjusted to cover almost the whole visible spectrum as shown in Fig. 1d.[46]

In pioneering work, $CH_3NH_3PbBr_3$ nanoparticles were exploited as the light sensitizer for use in iodide/triiodide liquid electrolyte-based DSSCs, exhibiting a low PCE of 3.1% yet an attractively high open circuit voltage, V_{oc}, of 0.96 V.[47] Since then, the photovoltaic efficiency of $CH_3NH_3PbX_3$-based perovskite solar cells has been rapidly increased,[48] which can be ascribed to the effective integration of advantageous attributes of $CH_3NH_3PbX_3$ nanocrystals (*i.e.*, direct band gap, high absorption and high carrier mobility) with the innovation of device architectures.[49] Compared to the complex chemistry of organic dyes, perovskite sensitizers can be readily synthesized through intrinsic ionic interaction of perovskite precursors (*e.g.*, CH_3NH_3I and PbI_2).[46] The relatively low-lying valence band of perovskite $CH_3NH_3PbBr_3$ renders high V_{oc} exceeding 1 V in DSSCs.[50] In addition, perovskite materials exhibit high absorption coefficient, large charge carrier mobility, and enhanced stability, which are expected to effectively promote photovoltaic efficiency, avoid liquid-electrolyte leakage, and improve device durability of DSSCs. In this Feature Article, we summarize the recent incredible achievements in perovskite solar cells, highlight the strategies of implementing solid-state HTMs, modified TiO_2 nanostructures and new device architectures to promote the photovoltaic performance, and provide an outlook on the future development of high efficiency perovskite solar cells.

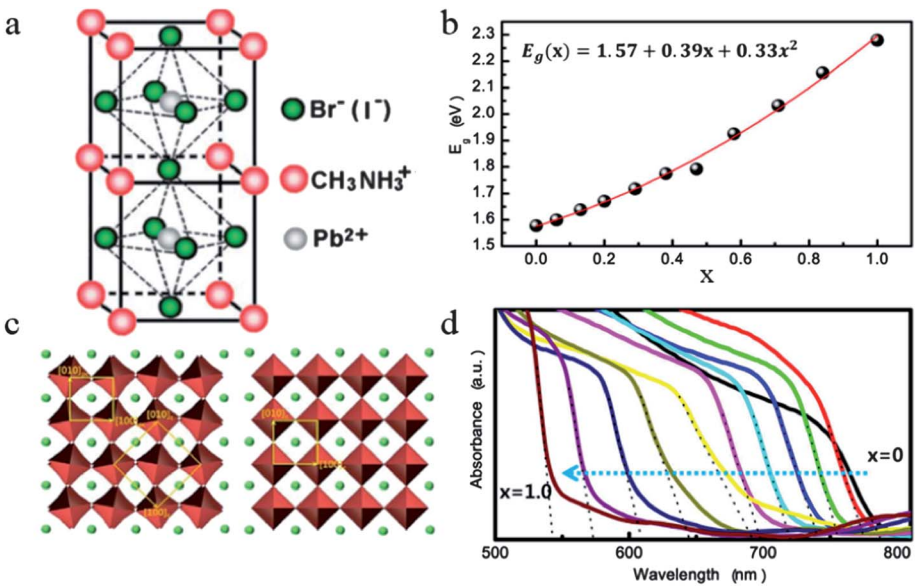

Fig. 1 (a) Crystal structure of organolead halide perovskites.[45] (b) The bandgaps of $CH_3NH_3Pb(I_{1-x}Br_x)_3$ as a function of Br composition, *x*. (c) Crystal structures and unit lattice vectors on the (00l) plane of the tetragonal (*I*4/*mcm*) (left) and cubic ($Pm\bar{3}m$) (right) phases. (d) UV-vis absorption spectra of $CH_3NH_3Pb(I_{1-x}Br_x)_3$.[46] Adapted with permission from ref. 45 and 46, Copyright© 2013 Royal Society of Chemistry, and © 2013 American Chemistry Society.

2. Perovskite-sensitized solar cells

2.1 Solid-state HTMs as electrolytes

Perovskite $CH_3NH_3PbI_3$ nanocrystals were initially used to enhance the light absorption of DSSCs employing liquid electrolytes, resulting in a highest PCE of 3.8% with a maximum IPCE of 45% in the wavelength region between 400 nm and 600 nm.[47] The PCE of $CH_3NH_3PbI_3$-sensitized DSSCs was then increased to 6.2% by the utilization of $CH_3NH_3PbI_3$ quantum dots (QDs), in which perovskite QDs were directly prepared from their precursor solution consisting of a mixture of CH_3NH_3I and PbI_2 in γ-butyrolactone, followed by the deposition on the mesoporous TiO_2 photoanode.[51] The electron diffusion coefficient of the perovskite QD-sensitized TiO_2 photoanode was higher than that of the organic dye N719-sensitized TiO_2 photoanode, suggesting that more photo-injected electrons can be generated in perovskite QD-sensitized DSSCs.[52] On the other hand, it was found that $CH_3NH_3PbI_3$ QDs could hardly cover the entire surface of the TiO_2 photoanode, and the exposure of the partial photoanode surface to the liquid electrolyte led to an increased electron recombination.[51] Such an electron recombination was reduced by modifying the TiO_2 surface with $Pb(NO_3)_2$ prior to the deposition of $CH_3NH_3PbI_3$ QDs, resulting in a slight increase in PCE (from 6.2% to 6.5%) with a maximum EQE of 78.6% at the wavelength of 530 nm.[51]

Although the PCE of perovskite QD-sensitized DSSCs reached over 6%, the V_{oc} was still comparable with that of conventional organic dye-sensitized DSSCs in the range of 0.6–0.8 V. The V_{oc} of DSSCs is mainly determined by the difference between the quasi Fermi level of the TiO_2 photoanode and the redox potential of the electrolyte.[53,54] In comparison to the conventional iodide/triiodide liquid electrolyte, solid-state HTMs were shown to increase the V_{oc} of as-prepared DSSCs due to their high redox potential.[10,55] In addition to the increased V_{oc}, the replacement of the liquid electrolyte with solid-state HTMs is also expected to improve the stability of perovskite $CH_3NH_3PbI_3$-sensitized DSSCs as $CH_3NH_3PbI_3$ nanocrystals were found to degrade in liquid electrolytes.[56]

The solid-state HTM spiro-MeOTAD has been widely recognized as an attractive alternative to the conventional iodide/triiodide liquid electrolyte in DSSCs. This is due to the redox potential of spiro-MeOTAD fits better with organic dyes, resulting in a remarkably high V_{oc} of 1.02 V.[57] The unexpected low PCEs of spiro-MeOTAD-based DSSCs using organic dyes as sensitizers can be attributed to the incomplete pore filling of dye-sensitized mesoporous TiO_2 films with solid-state HTMs, which heavily limits the applicable thickness of TiO_2 films, and in turn the amount of dye loading and the light-harvesting efficiency, and ultimately the device performance.[58,59] However, for perovskite $CH_3NH_3PbI_3$-sensitized DSSCs, a thin perovskite–TiO_2 film can readily harvest enough photons to generate a high short-circuit photocurrent density, J_{sc}, which can be attributed to the particularly high absorption coefficient of $CH_3NH_3PbI_3$ nanocrystals. In this context, the highest PCE of $CH_3NH_3PbI_3$-sensitized DSSCs was strikingly increased from 6.5% to 9.7% by employing spiro-MeOTAD HTM instead of liquid electrolytes (Fig. 2), in which the thickness of the TiO_2 photoanode (*i.e.*, 0.6 μm) was much thinner than that in previous work.[56]

It is noteworthy that the photovoltaic performance of $CH_3NH_3PbI_3$-sensitized DSSCs can be significantly promoted by sequential deposition of perovskite $CH_3NH_3PbI_3$ nanocrystals on mesoporous TiO_2 films, which leads to a high loading and coverage of perovskite nanocrystals on the TiO_2 photoanode surface. The mesoporous TiO_2 films were initially infiltrated in a high concentration of PbI_2/*N*,*N*-dimethylformamide solution to achieve a high loading of PbI_2 nanocrystals within mesoporous TiO_2 films (Fig. 3a), followed by the immersion of TiO_2/PbI_2 films in CH_3NH_3I/2-propanol solution to form densely packed $CH_3NH_3PbI_3$ nanocrystals on TiO_2 films (Fig. 3b).[60] The confinement of PbI_2 nanocrystals within mesoporous TiO_2 films resulted in a layered PbI_2 crystalline structure, which is expected to greatly facilitate the insertion of CH_3NH_3I precursors to yield $CH_3NH_3PbI_3$ nanocrystals.[61,62] The highest PCE of the as-prepared DSSCs up to 15% with a long-term stability of maintaining 80% of the initial PCE after 500 h (Fig. 3c) was obtained,[60] which is the known best performance DSSC.

2.2 TiO_2 nanostructures as the photoanode

As described above, mesoporous TiO_2 films composed of randomly dispersed TiO_2 nanoparticle networks are extensively employed as the photoanode in both liquid-electrolyte- and solid-state-based DSSCs because of their excellent physicochemical properties such as appropriate electronic band structure, chemical stability, photostability, non-toxicity, and low cost, in conjunction with the large surface area provided by the mesoporous network structure for sufficient dye loading.[63,64] To date, the highest PCEs of 10.2% and 15% have been achieved in the TiO_2/N719/perovskite $CsSnI_3$ and TiO_2/$CH_3NH_3PbI_3$/spiro-MeOTAD DSSCs, respectively.[60,65] However, the device performance of DSSCs is limited by the electron trapping and scattering at the grain boundary of the TiO_2 nanoparticle network. In comparison to the high charge recombination loss in mesoporous TiO_2 nanoparticle films, vertically aligned one-dimensional (1D) TiO_2 nanostructures, such as nanorods, nanowires, and nanotubes, have been demonstrated to provide a better pathway along the long axis of 1D nanostructures for electron transport, thereby imparting longer electron lifetime, reducing charge recombination at grain boundary, and enhancing the device efficiency of conventional liquid-electrolyte-based DSSCs.[22,24,63]

1D oriented TiO_2 nanowire arrays can be directly seeded and grown on FTO electrodes by the hydrothermal reaction, in which the lattice mismatch between the FTO substrate and rutile TiO_2 acts as the major driving force for the nucleation and growth of rutile TiO_2 nanorods.[66] A highest PCE of 4.87% was obtained when depositing perovskite $CH_3NH_3PbI_2Br$ nanocrystals on the TiO_2 nanowire arrays with the nanowire diameter of 50–150 nm and the array thickness of ~1.5 μm.[67] The relatively low PCE was correlated with the previous work using mesoporous TiO_2 nanocrystal films, signifying that an optimized thickness for the TiO_2 photoanode would be less than 1 μm for perovskite-sensitized DSSCs, considering that

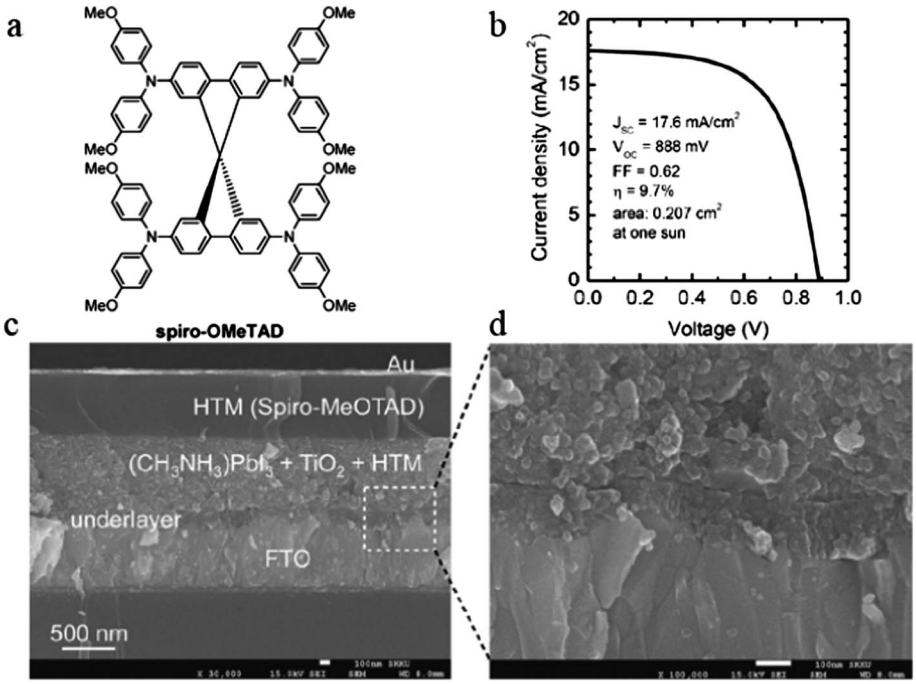

Fig. 2 (a) Chemical structure of 2,2′,7,7′-tetrakis-(*N*,*N*-di-*p*-methoxyphenylamine)-9,9′-spirobifluorene (spiro-MeOTAD). (b) Current density–voltage (*J*–*V*) curve of perovskite $CH_3NH_3PbI_3$-sensitized DSSCs using spiro-MeOTAD as the hole-transport material. (c) Cross-sectional SEM image of the device. (d) Close-up of an active layer–underlayer–FTO interfacial junction structure.[56] Adapted with permission from ref. 56, Copyright© 2012 Nature Publishing Group.

the TiO_2 photoanode needs to be thick enough to adsorb more dyes yet be thin enough to facilitate the charge carrier transport.[56]

The thickness effect of the nanostructured TiO_2 photoanode on the photovoltaic performance of perovskite $CH_3NH_3PbI_3$-sensitized DSSCs was studied by exploiting oriented TiO_2

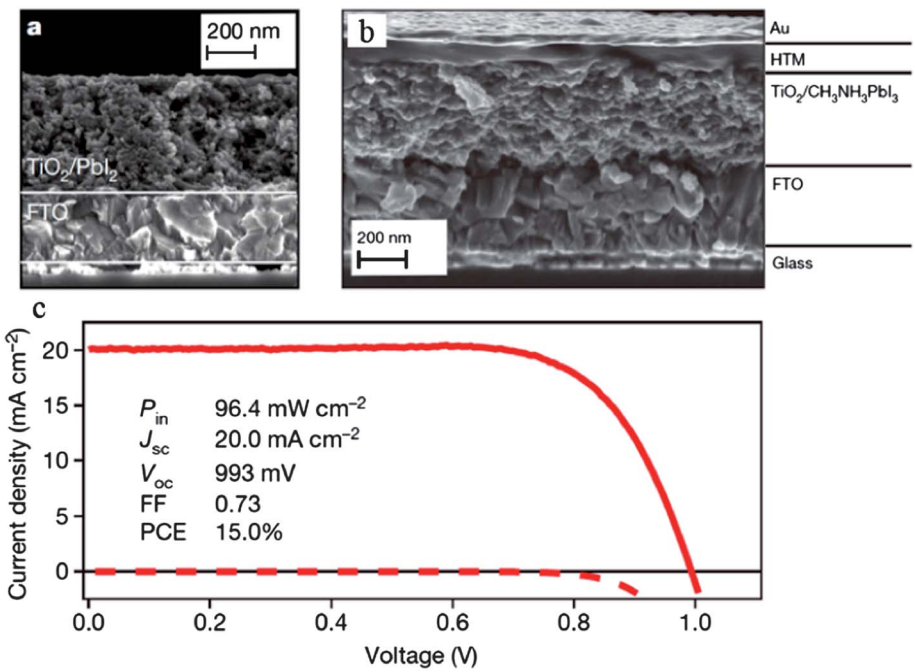

Fig. 3 (a) Cross-sectional SEM of a mesoporous TiO_2 film infiltrated with PbI_2. (b) Cross-sectional SEM of a complete photovoltaic device. (c) Current density–voltage (*J*–*V*) curve of a best-performing cell measured at a simulated AM 1.5G solar irradiation of 96.4 mW cm^{-2} (solid line) and in the dark (dashed line).[60] Adapted with permission from ref. 60, Copyright© 2013 Nature Publishing Group.

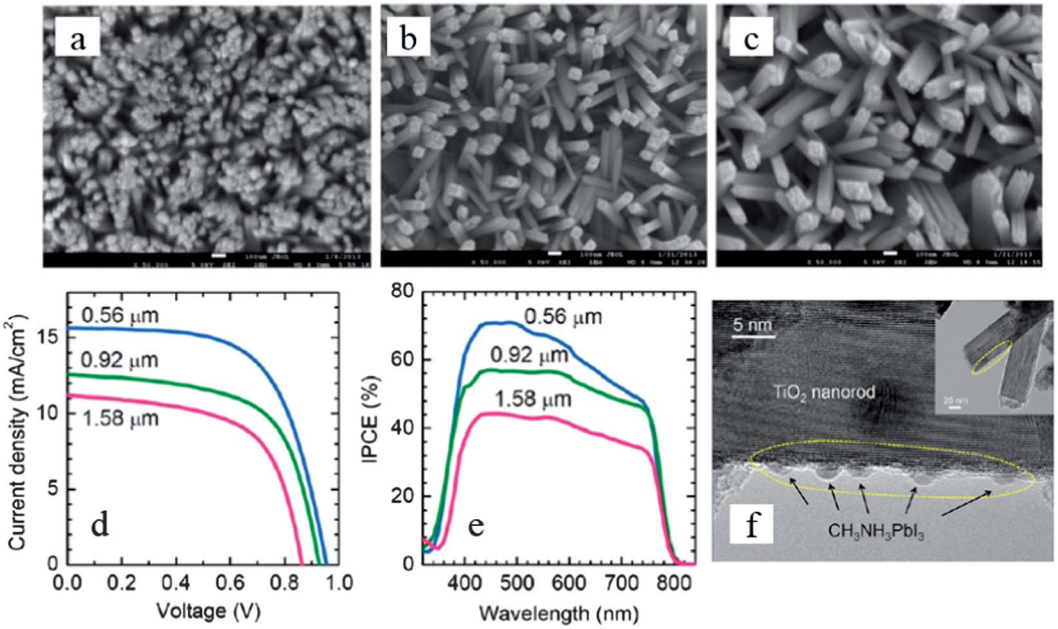

Fig. 4 (a–c) FESEM images of rutile TiO_2 nanorods grown on the FTO substrate (top views). (d–e) Effect of the length of TiO_2 nanorods on (d) current density–voltage (*J*–*V*) curves and (e) IPCE in a solid-state DSSC based on $CH_3NH_3PbI_3$-sensitized rutile TiO_2 nanorods and spiro-MeOTAD. (f) TEM micrograph of $CH_3NH_3PbI_3$ deposited on the surface of TiO_2 nanorods.[68] Adapted with permission from ref. 68, Copyright© 2013 American Chemical Society.

nanorod arrays as the photoanode. The rutile TiO_2 nanorod arrays with the thicknesses of ~0.56 μm, ~0.92 μm, and ~1.58 μm were uniformly grown on FTO electrodes (Fig. 4a–c), respectively.[68] The decreases of J_{sc} and IPCE were observed with the increased TiO_2 thicknesses, which was related to the increased tilting angles for longer nanorods, corresponding to the reduced pore filling fraction of perovskite sensitizers and thus low light-harvesting efficiencies (Fig. 4d and e).[68] Thus, the highest PCE of 9.4% was obtained with the smallest thickness of ~0.56 μm. It is worth noting that the TiO_2 nanorod surface was incompletely covered with the perovskite nanoparticles (Fig. 4f).[68] Further efforts to increase the surface area for dye adsorption within the 1D nanostructured TiO_2 and reduce the shunt current are required in the future research.

3. Planar heterojunction perovskite solar cells

Quite intriguingly, the PCE of perovskite $CH_3NH_3PbI_2Cl$-sensitized DSSCs unexpectedly reached 10.9% with a high V_{oc} of 0.98 V by replacing the conventional mesoporous TiO_2 film with the mesoporous Al_2O_3 film.[23] Considering the insulating nature of Al_2O_3, the photo-generated electrons in Al_2O_3-based devices must be confined within the perovskite $CH_3NH_3PbI_2Cl$ phase before they are collected by the bottom FTO electrode,[69] indicating that the electrons are able to transport through the $CH_3NH_3PbI_2Cl$ phase without significant charge recombination (Fig. 5).[23] In fact, a higher electron diffusion rate was found in the $CH_3NH_3PbI_2Cl$ phase than that in mesoporous TiO_2 films, revealing that the perovskite $CH_3NH_3PbI_2Cl$ possesses an ambipolar transport property.[23] The confinement of photogenerated electrons within the perovskite $CH_3NH_3PbI_2Cl$ phase is believed to play a crucial role in enhancing the V_{oc} to 0.98 V *via* increasing the splitting of the quasi-Fermi levels of electrons and holes within the $CH_3NH_3PbI_2Cl$ phase, as the V_{oc} is determined by the difference of the quasi-Fermi levels within the absorber layer.[70] The device efficiency was further improved to 12.3% by optimizing the film thickness of the Al_2O_3 layer,[71] strongly suggesting that the perovskite $CH_3NH_3PbX_3$ (X = halogen) actually serves as not only a light sensitizer but also a semiconducting active layer, in which the photogenerated charge carriers are efficiently transported to the top and bottom electrodes, respectively, through the $CH_3NH_3PbX_3$ (X = halogen) phase.

Similar evidence of the semiconducting diode properties of perovskite $CH_3NH_3PbX_3$ was somewhat observed in exploring their use as light sensitizers in DSSCs.[23,67] Although the solid-state Au/$CH_3NH_3PbX_3$/TiO_2 heterojunction solar cell exhibited a very low PCE of 5.5%, its maximum IPCE can reach as high as 90% in the visible light range, corresponding to a high J_{sc} of 16.1 mA cm^{-2}.[49] This signified that the perovskite $CH_3NH_3PbX_3$ could probably work as the photovoltaic active layer in the architecture of planar heterojunction solar cells. The relatively low V_{oc}, FF, and thus PCE of the perovskite-based planar heterojunction solar cells may be increased by optimizing the film morphology of the perovskite active layer to achieve a pinhole-free layer, avoid short circuit, and increase shunt resistance.[70]

Quite recently, Snaith and his coworkers demonstrated that high performance perovskite $CH_3NH_3PbX_3$ (X = halogen) solar cells can indeed be fabricated in a simple planar heterojunction architecture instead of complex nanostructured DSSCs. They

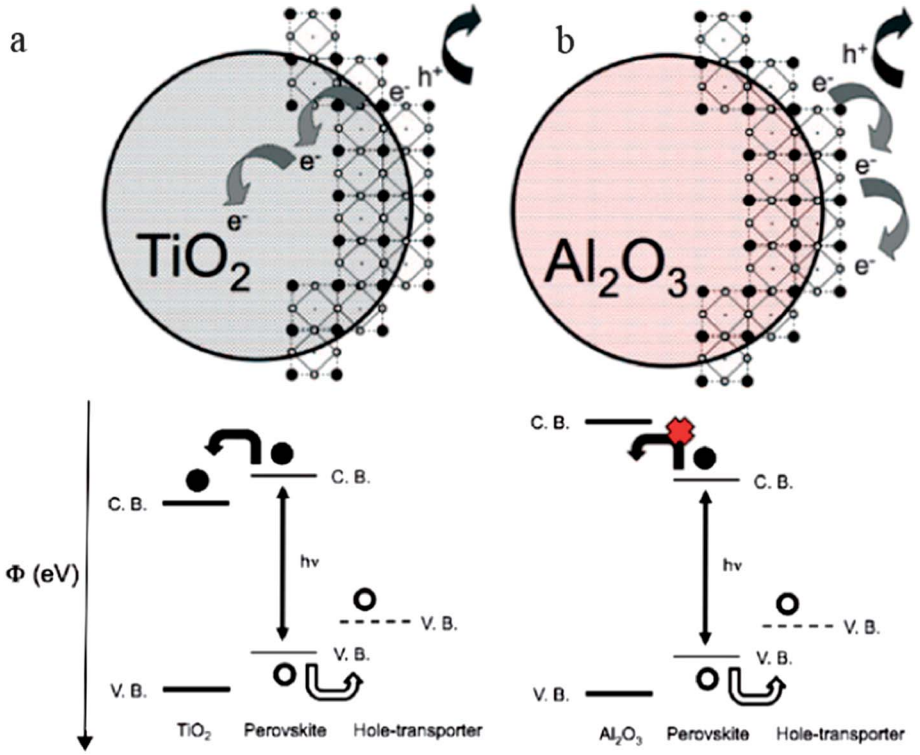

Fig. 5 Schematic illustration of charge transfer and charge transport in (a) a perovskite-sensitized TiO_2 solar cell and (b) an insulating Al_2O_3-based solar cell. The corresponding representation of the energy landscape is shown below in which electrons and holes are shown as solid circles and open circles, respectively.[23] Adapted with permission from ref. 23, Copyright© 2012 American Association for the Advancement of Science.

also scrutinized the effects of the perovskite film morphology on the device performance. The planar heterojunction perovskite solar cells were fabricated in a configuration of FTO/compact TiO_2/$CH_3NH_3Pb(I_{1-x}Cl_x)_3$ ($0 \leq x \leq 1$)/spiro-MeOTAD/Au,[72] wherein FTO is the transparent bottom electrode, compact TiO_2 is the hole-blocking layer, $CH_3NH_3Pb(I_{1-x}Cl_x)_3$ is the active layer, spiro-MeOTAD is the electron-blocking layer, and Au is the top electrode. The device performance was found to depend heavily on the coverage of $CH_3NH_3Pb(I_{1-x}Cl_x)_3$ on the compact TiO_2 layer (Fig. 6),[72] in which a high $CH_3NH_3Pb(I_{1-x}Cl_x)_3$ coverage was usually preferred for high J_{sc} and PCE. This is because the insufficient coverage would form shunt paths between the top and bottom electrodes, resulting in the decreased V_{oc} and FF. In the solution-processed fabrication, a high coverage was achieved by optimizing the film thickness, thermal annealing temperature, and thermal annealing time of the perovskite films,[72] yielding a high PCE of 11.4%.

The development of an effective film deposition technique and an interface engineering procedure is of great importance for thin-film solar cells, as it facilitates the reduction of the loss of light absorption, the decrease of shunt paths, and the minimization of the interface-defect density in planar heterojunction solar cells.[70] To this end, the vapour deposition was employed to coat a perovskite $CH_3NH_3Pb(I_{1-x}Cl_x)_3$ film on a compact TiO_2 layer, forming a superior uniform layer of $CH_3NH_3Pb(I_{1-x}Cl_x)_3$ films as compared to the incomplete

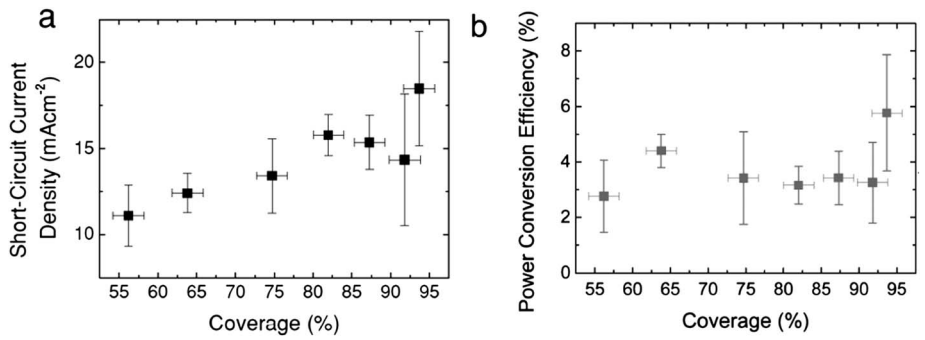

Fig. 6 The relationships between (a) the short-circuit current density (J_{sc}) and the perovskite coverage; and (b) the power conversion efficiency (PCE) and the perovskite coverage.[72] Adapted with permission from ref. 72, Copyright© 2013 Wiley-VCH.

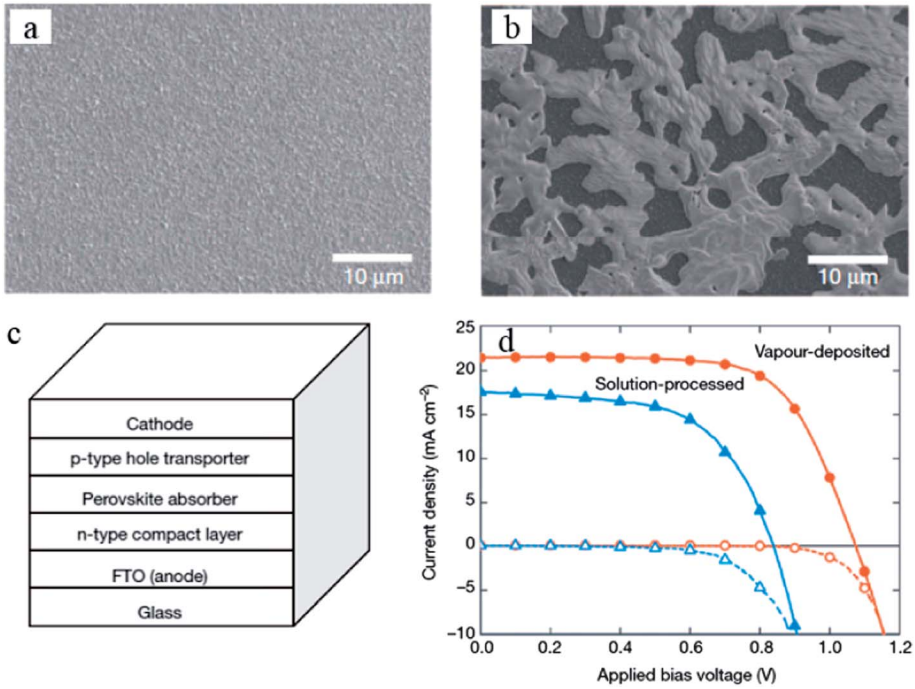

Fig. 7 SEM images of (a) a vapour-deposited perovskite film and (b) a solution-processed perovskite film (top views). (c) Schematic of a planar heterojunction p–i–n perovskite solar cell. (d) Current density–voltage (J–V) curves of the best-performing solution-processed (blue lines, triangles) and vapour-deposited (red lines, circles) planar heterojunction perovskite solar cells measured under simulated AM 1.5 sunlight of 101 mW cm^{-2} irradiance (solid lines) and in the dark (dashed lines).[73] Adapted with permission from ref. 73, Copyright© 2013 Nature Publishing Group.

coverage of $CH_3NH_3Pb(I_{1-x}Cl_x)_3$ platelets prepared by the solution-processed method (Fig. 7a and b).[73] In an optimized device with the vapour-deposited $CH_3NH_3Pb(I_{1-x}Cl_x)_3$ as an active layer, the planar heterojunction perovskite solar cells yielded an extremely high J_{sc} of 21.5 mA cm^{-2}, V_{oc} of 1.07 V, FF of 0.67, and PCE of 15.4% (Fig. 7c and d),[73] which exceeded the highest PCEs of conventional liquid-electrolytes and perovskite-sensitized DSSCs.[10,60] Clearly, the judicious integration of the unique photovoltaic performance of perovskite materials, the simple planar heterojunction architecture, and the vapour deposition make the exploration of perovskite solar cells stand out as the promising and bright direction for achieving high performance next generation solar cells at competitively low cost.

4. Conclusions and outlook

The past few years have witnessed unprecedented rapid progress in the development of perovskite solar cells.[47] Two research groups, Grätzel and Snaith, have made impressive contributions to increasing the photovoltaic performance and innovating the device architecture of perovskite solar cells. Perovskite nanocrystals were initially used as high-efficiency light sensitizers in iodide/triiodide liquid-electrolyte-based DSSCs due to their direct semiconducting nature, high light absorption, and fast carrier mobility,[47] yet the PCEs of which were lower than those organic dye-sensitized DSSCs. The replacement of the iodide/triiodide liquid electrolyte with the solid-state spiro-MeOTAD HTM profoundly increased the PCEs of perovskite-sensitized DSSCs from ~6% up to 10% with enhanced device stability.[56] Remarkably, the PCEs have been recently promoted to ~15% by increasing the loading concentration of perovskite sensitizers within mesoporous TiO_2 films *via* the sequential deposition of perovskite nanocrystals,[60] representing to date the highest PCE for DSSCs.

The success of employing perovskite materials in DSSCs invokes great interest in exploring their working mechanism. Intriguingly, more evidence has revealed that the perovskite can not only act as a high efficiency light absorber but also possess excellent charge carrier mobility.[71,72] The perovskite has unique ambipolar properties to transport both photogenerated holes and electrons. In this context, a simple planar heterojunction configuration composed of FTO/compact TiO_2/perovskite/HTM/Au was successfully employed to fabricate perovskite solar cells, dispensing with the need for complex DSSC architectures.[73] The PCEs of the as-prepared perovskite solar cells exceeded 15%, making it stand out as an unambiguously attractive route to low cost and high performance next generation solar cells.

Despite the exciting high efficiency over 15% in the planar heterojunction perovskite solar cells, the performance of perovskite solar cells is envisioned to further improve up to 20% by optimizing the planar heterojunction device configuration.[42] For the J_{sc}, the thickness of the perovskite active layer must be thick enough to absorb sufficient incident light, while at the same time a thick film is not favorable for the charge carrier diffusion.[70] The optimization of the film morphology of the active layer, in particular the film thickness, roughness, and coverage, has been proved to be of key importance in producing

high performance perovskite solar cells. In addition, the implementation of antireflection or plasmonic technologies may also improve the efficiency of light harvesting, the J_{sc}, and thus the device performance. The interfacial layer between the perovskite active layer and the bottom (or top) electrode also needs to be rationally engineered, in which the interfacial defect density should be minimized and the energy levels need to be closely aligned in order to achieve high V_{oc} and FF.

Given the relatively short period of time in developing perovskite solar cells, the fundamental working mechanisms of perovskite in either DSSCs or planar heterojunction solar cells are still not well understood. Further elucidation on photophysical properties of perovskite materials will be highly beneficial to improving device performance of perovskite solar cells. Furthermore, the most widely studied perovskite material for solar cells at present is $CH_3NH_3PbX_3$. It may be highly desirable to replace the toxic Pb cations with other environmentally friendly elements. The water-soluble property of $CH_3NH_3PbX_3$ is preferred for the chemical synthesis but not for the device stability.[74] Clearly, all these issues described above should be centered on the exploration of perovskite materials for low cost, high efficiency perovskite solar cells. Nonetheless, with recent progress being made in chemical synthesis, device engineering, film deposition, and theoretical modeling, the field of perovskite solar cells should have a bright, rapidly evolving and practical future.

Acknowledgements

We gratefully acknowledge funding support from the Air Force Office of Scientific Research (FA9550-13-1-0101).

References

1 A. Shah, P. Torres, R. Tscharner, N. Wyrsch and H. Keppner, *Science*, 1999, **285**, 692.
2 W. U. Huynh, J. J. Dittmer and A. P. Alivisatos, *Science*, 2002, **295**, 2425.
3 G. Li, V. Shrotriya, J. S. Huang, Y. Yao, T. Moriarty, K. Emery and Y. Yang, *Nat. Mater.*, 2005, **4**, 864.
4 A. Hagfeldt, G. Boschloo, L. C. Sun, L. Kloo and H. Pettersson, *Chem. Rev.*, 2010, **110**, 6595.
5 M. He, F. Qiu and Z. Q. Lin, *J. Mater. Chem.*, 2011, **21**, 17039.
6 M. He, W. Han, J. Ge, Y. L. Yang, F. Qiu and Z. Q. Lin, *Energy Environ. Sci.*, 2011, **4**, 2894.
7 A. Bhuwalka, J. F. Mike, M. He, J. J. Intemann, T. Nelson, M. D. Ewan, R. A. Roggers, Z. Q. Lin and M. Jeffries-El, *Macromolecules*, 2011, **44**, 9611.
8 M. He, F. Qiu and Z. Q. Lin, *J. Phys. Chem. Lett.*, 2013, **4**, 1788.
9 M. A. Green, K. Emery, Y. Hishikawa, W. Warta and E. D. Dunlop, *Prog. Photovoltaics*, 2012, **20**, 606.
10 A. Yella, H. W. Lee, H. N. Tsao, C. Yi, A. K. Chandiran, M. K. Nazeeruddin, E. W. Diau, C. Y. Yeh, S. M. Zakeeruddin and M. Grätzel, *Science*, 2011, **334**, 629.
11 H. J. Xiang, B. Huang, E. J. Kan, S. H. Wei and X. G. Gong, *Phys. Rev. Lett.*, 2013, **110**, 118702.
12 K. L. Chopra, P. D. Paulson and V. Dutta, *Prog. Photovoltaics*, 2004, **12**, 69.
13 J. Britt and C. Ferekides, *Appl. Phys. Lett.*, 1993, **62**, 2851.
14 M. A. Contreras, B. Egaas, K. Ramanathan, J. Hiltner, A. Swartzlander, F. Hasoon and R. Noufi, *Prog. Photovoltaics*, 1999, **7**, 311.
15 Q. J. Guo, H. W. Hillhouse and R. Agrawal, *J. Am. Chem. Soc.*, 2009, **131**, 11672.
16 B. Oregan and M. Grätzel, *Nature*, 1991, **353**, 737.
17 L. M. Goncalves, V. D. Bermudez, H. A. Ribeiro and A. M. Mendes, *Energy Environ. Sci.*, 2008, **1**, 655.
18 M. Grätzel, *J. Photochem. Photobiol., C*, 2003, **4**, 145.
19 A. B. F. Martinson, T. W. Hamann, M. J. Pellin and J. T. Hupp, *Chem.–Eur. J.*, 2008, **14**, 4458.
20 S. Yanagida, Y. H. Yu and K. Manseki, *Acc. Chem. Res.*, 2009, **42**, 1827.
21 J. N. Clifford, E. Martinez-Ferrero, A. Viterisi and E. Palomares, *Chem. Soc. Rev.*, 2011, **40**, 1635.
22 J. Wang and Z. Q. Lin, *Chem.–Asian J.*, 2012, **7**, 2754.
23 M. M. Lee, J. Teuscher, T. Miyasaka, T. N. Murakami and H. J. Snaith, *Science*, 2012, **338**, 643.
24 M. D. Ye, H. Y. Liu, C. J. Lin and Z. Q. Lin, *Small*, 2013, **9**, 312.
25 Y. H. Jang, X. K. Xin, M. Byun, Y. J. Jang, Z. Q. Lin and D. H. Kim, *Nano Lett.*, 2012, **12**, 479.
26 X. K. Xin, M. He, W. Han, J. H. Jung and Z. Q. Lin, *Angew. Chem., Int. Ed.*, 2011, **50**, 11739.
27 G. G. Xue, Y. Guo, T. Yu, J. Guan, X. R. Yu, J. Y. Zhang, J. G. Liu and Z. G. Zou, *Int. J. Electrochem. Sci.*, 2012, **7**, 1496.
28 R. Kern, N. Van Der Burg, G. Chmiel, J. Ferber, G. Hasenhindl, A. Hinsch, R. Kinderman, J. Kroon, A. Meyer, T. Meyer, R. Niepmann, J. Van Roosmalen, C. Schill, P. Sommeling, M. Spath and I. Uhlendorf, *Opto-Electron. Rev.*, 2000, **8**, 284.
29 P. M. Sommeling, M. Spath, H. J. P. Smit, N. J. Bakker and J. M. Kroon, *J. Photochem. Photobiol., A*, 2004, **164**, 137.
30 H. X. Wang, H. Li, B. F. Xue, Z. X. Wang, Q. B. Meng and L. Q. Chen, *J. Am. Chem. Soc.*, 2005, **127**, 6394.
31 J. N. de Freitas, A. F. Nogueira and M. A. De Paoli, *J. Mater. Chem.*, 2009, **19**, 5279.
32 M. Wang, X. Pan, X. Q. Fang, L. Guo, W. Q. Liu, C. N. Zhang, Y. Huang, L. H. Hu and S. Y. Dai, *Adv. Mater.*, 2010, **22**, 5526.
33 U. Bach, D. Lupo, P. Comte, J. E. Moser, F. Weissortel, J. Salbeck, H. Spreitzer and M. Grätzel, *Nature*, 1998, **395**, 583.
34 N. Cai, S. J. Moon, L. Cevey-Ha, T. Moehl, R. Humphry-Baker, P. Wang, S. M. Zakeeruddin and M. Grätzel, *Nano Lett.*, 2011, **11**, 1452.
35 J. H. Wu, S. Hao, Z. Lan, J. M. Lin, M. L. Huang, Y. F. Huang, P. J. Li, S. Yin and T. Satot, *J. Am. Chem. Soc.*, 2008, **130**, 11568.
36 J. K. Koh, J. Kim, B. Kim, J. H. Kim and E. Kim, *Adv. Mater.*, 2011, **23**, 1641.
37 G. K. Mor, S. Kim, M. Paulose, O. K. Varghese, K. Shankar, J. Basham and C. A. Grimes, *Nano Lett.*, 2009, **9**, 4250.
38 J. A. Chang, J. H. Rhee, S. H. Im, Y. H. Lee, H. J. Kim, S. I. Seok, M. K. Nazeeruddin and M. Grätzel, *Nano Lett.*, 2010, **10**, 2609.

39 J. J. Sun and E. M. Goldys, *J. Phys. Chem. C*, 2008, **112**, 9261.
40 B. Hanewinkel, A. Knorr, P. Thomas and S. W. Koch, *Phys. Rev. B: Condens. Matter Mater. Phys.*, 1997, **55**, 13715.
41 D. Q. Bi, L. Yang, G. Boschloo, A. Hagfeldt and E. M. J. Johansson, *J. Phys. Chem. Lett.*, 2013, **4**, 1532.
42 N. G. Park, *J. Phys. Chem. Lett.*, 2013, **4**, 2423.
43 W. F. Forrester and R. M. Hinde, *Nature*, 1945, **156**, 177.
44 H. D. Megaw, *Nature*, 1945, **155**, 484.
45 B. Cai, Y. D. Xing, Z. Yang, W. H. Zhang and J. S. Qiu, *Energy Environ. Sci.*, 2013, **6**, 1480.
46 J. H. Noh, S. H. Im, J. H. Heo, T. N. Mandal and S. I. Seok, *Nano Lett.*, 2013, **13**, 1764.
47 A. Kojima, K. Teshima, Y. Shirai and T. Miyasaka, *J. Am. Chem. Soc.*, 2009, **131**, 6050.
48 J. Bisquert, *J. Phys. Chem. Lett.*, 2013, **4**, 2597.
49 L. Etgar, P. Gao, Z. S. Xue, Q. Peng, A. K. Chandiran, B. Liu, M. K. Nazeeruddin and M. Grätzel, *J. Am. Chem. Soc.*, 2012, **134**, 17396.
50 E. Edri, S. Kirmayer, D. Cahen and G. Hodes, *J. Phys. Chem. Lett.*, 2013, **4**, 897.
51 J. H. Im, C. R. Lee, J. W. Lee, S. W. Park and N. G. Park, *Nanoscale*, 2011, **3**, 4088.
52 A. J. Frank, N. Kopidakis and J. van de Lagemaat, *Coord. Chem. Rev.*, 2004, **248**, 1165.
53 T. Daeneke, A. J. Mozer, Y. Uemura, S. Makuta, M. Fekete, Y. Tachibana, N. Koumura, U. Bach and L. Spiccia, *J. Am. Chem. Soc.*, 2012, **134**, 16925.
54 T. Daeneke, A. J. Mozer, T. H. Kwon, N. W. Duffy, A. B. Holmes, U. Bach and L. Spiccia, *Energy Environ. Sci.*, 2012, **5**, 7090.
55 J. Burschka, A. Dualeh, F. Kessler, E. Baranoff, N. L. Cevey-Ha, C. Yi, M. K. Nazeeruddin and M. Grätzel, *J. Am. Chem. Soc.*, 2011, **133**, 18042.
56 H. S. Kim, C. R. Lee, J. H. Im, K. B. Lee, T. Moehl, A. Marchioro, S. J. Moon, R. Humphry-Baker, J. H. Yum, J. E. Moser, M. Grätzel and N. G. Park, *Sci. Rep.*, 2012, **2**, 591.
57 S. R. Jang, K. Zhu, M. J. Ko, K. Kim, C. Kim, N. G. Park and A. J. Frank, *ACS Nano*, 2011, **5**, 8267.
58 I. K. Ding, N. Tetreault, J. Brillet, B. E. Hardin, E. H. Smith, S. J. Rosenthal, F. Sauvage, M. Grätzel and M. D. McGehee, *Adv. Funct. Mater.*, 2009, **19**, 2431.
59 F. Fabregat-Santiago, J. Bisquert, L. Cevey, P. Chen, M. K. Wang, S. M. Zakeeruddin and M. Grätzel, *J. Am. Chem. Soc.*, 2009, **131**, 558.
60 J. Burschka, N. Pellet, S. J. Moon, R. Humphry-Baker, P. Gao, M. K. Nazeeruddin and M. Grätzel, *Nature*, 2013, **499**, 316.
61 H. Li, M. Zanella, A. Genovese, M. Povia, A. Falqui, C. Giannini and L. Manna, *Nano Lett.*, 2011, **11**, 4964.
62 G. I. Gurina and K. V. Savchenko, *J. Solid State Chem.*, 2004, **177**, 909.
63 M. D. Ye, X. K. Xin, C. J. Lin and Z. Q. Lin, *Nano Lett.*, 2011, **11**, 3214.
64 X. K. Xin, M. Scheiner, M. D. Ye and Z. Q. Lin, *Langmuir*, 2011, **27**, 14594.
65 I. Chung, B. Lee, J. Q. He, R. P. H. Chang and M. G. Kanatzidis, *Nature*, 2012, **485**, 486.
66 B. Liu and E. S. Aydil, *J. Am. Chem. Soc.*, 2009, **131**, 3985.
67 J. H. Qiu, Y. C. Qiu, K. Y. Yan, M. Zhong, C. Mu, H. Yan and S. H. Yang, *Nanoscale*, 2013, **5**, 3245.
68 H. S. Kim, J. W. Lee, N. Yantara, P. P. Boix, S. A. Kulkarni, S. Mhaisalkar, M. Grätzel and N. G. Park, *Nano Lett.*, 2013, **13**, 2412.
69 A. Kojima, M. Ikegami, K. Teshima and T. Miyasaka, *Chem. Lett.*, 2012, **41**, 397.
70 W. Jaegermann, A. Klein and T. Mayer, *Adv. Mater.*, 2009, **21**, 4196.
71 J. M. Ball, M. M. Lee, A. Hey and H. J. Snaith, *Energy Environ. Sci.*, 2013, **6**, 1739.
72 G. E. Eperon, V. M. Burlakov, P. Docampo, A. Goriely and H. J. Snaith, *Adv. Funct. Mater.*, 2013, DOI: 10.1002/adfm.201302090.
73 M. Liu, M. B. Johnston and H. J. Snaith, *Nature*, 2013, **501**, 395.
74 M. D. McGehee, *Nature*, 2013, **501**, 323.